

Betel Nut Shell Water Extract as a Green Corrosion Inhibitor for Q235 Steel in 1 M HCl

Zhao Zipeng¹, Yongbo Yan², Zhengyuan Gao^{3,*}

¹ College of Materials Science and Engineering, Chongqing University, Chongqing, 40045

² School of Oil and Natural Gas Engineering, Southwest Petroleum University, Chengdu 610500

³ School of Mechatronics & Vehicle Engineering, Chongqing Jiaotong University, Chongqing, 400074, China;

*E-mail: zhengyuangao@cqjtu.edu.cn (Z. Gao)

Received: 25 July 2022 / Accepted: 1 September 2022 / Published: 10 October 2022

In this work, we prepare the Betel nut shell extract (BNE) as an eco-friendly candidate to replace toxic and difficult to synthesize corrosion inhibitors. Combined with electrochemical tests, gravimetric measurements, morphology observations, adsorption curve, and theoretical calculations, the anti-corrosion ability and absorption mechanism of BNE on Q235 steel in 1 M HCl is explored. As shown in electrochemical results, BNE can reduce steel cathodic and anodic dissolution rates, and the highest η value is 93.1%. The high-efficiency inhibition ability corresponds to a stable and dense BNE film assembled between the HCl/steel substrate interface. Theoretical calculations further reveal the possibility of BNE molecules' parallel adsorption on the steel surface from the molecular level. Ultimately, this work can accumulate experience for the industrial application of plant extractant corrosion inhibitors.

Keywords: Plant extraction, Corrosion inhibitor, Steel, Electrochemical technology, Theoretical calculation

1. INTRODUCTION

Metal corrosion occurs all the time and everywhere. Damaged and scrapped instruments, equipment, bridges, platforms, and metallic materials due to metal corrosion are widespread. Metal corrosion can bring substantial economic losses and severe safety accidents [1-3]. In addition, corrosion of metals is more common and severe in some harsh acidic environments, such as sulfuric acid, hydrochloric acid, and nitric acid. According to relevant reports [4], the economic losses caused by corrosion in China exceeded 300 billion US dollars in 2014. The research on inhibiting metal corrosion is of great significance. Corrosion inhibitor is an economical, convenient, and efficient method in anti-

corrosion technologies [5-7]. Corrosion inhibitors are widely used in industrial water circulation systems and pickling systems.

Inorganic inhibitors include zinc salts, cerium salts, molybdates, chromates, nitrites, and phosphates, inhibiting metal dissolution by building a passivation film. However, the disadvantages of inorganic corrosion inhibitors are also evident, such as large dosages and being unfriendly to the environment [8]. Common organic corrosion inhibitors include imidazoles, thiazoles, triazoles, and tetrazoles [9]. An organic film is fabricated based on double /triple bonds, benzene ring, and heteroatoms (N, S, O, P) [10]. It is worth noting that the delocalized electron cloud and lone pair electrons of organic molecules are different, meaning the difference in adsorption performance. Qiang [11] explored the corrosion inhibition performance of 5-(Benzylthio)-1H-tetrazole (BTTA) and 5-Benzyl-1H-Tetrazole (BTA) on Q235 steel in sulfuric acid solution. Based on its S-linker, BTTA (98.3%) displayed an excellent anti-corrosion capacity than BTA (21.6%). However, poor water solubility and complicated synthesis steps restrict organic inhibitor development [12]. Therefore, developing eco-friendly, water-soluble, and readily available corrosion inhibitors has become a research hotspot.

Plant extracts (PE) are potential green corrosion inhibitors due to their advantages of vast sources, renewable, easy access, eco-friendly, biodegradability, and rich ingredients [13]. Researchers have made a lot of efforts on plant extracts as corrosion inhibitors. Li [14] investigated the anti-corrosion ability of *Brassica oleracea L* extracts (BOLE) on Q235 steel in acidic solutions. Based on experimental results and theoretical calculations, the authors found that BOLE displayed high-efficiency inhibition capacities (92.3% in 0.5 M H₂SO₄ and 93.8% in 1 M HCl) in two harsh acid environments. Bahlakeh [15] proved that *Peganum harmala seed* extract was an eco-friendly inhibitor for mild steel in HCl solution. Based on theoretical calculations, the authors explained the adsorption mechanism of the active ingredients in *Peganum harmala seed* extract on the mild steel surface. However, it is still significant to carry out basic research before the industrial application of plant extractant corrosion inhibitors.

Betel nut shell (Latin name *Pericarpium Arecae*) is used to treat diseases and cook dishes due to its wide range of sources, large yields, and easy access. Here, betel nut shell extract (BNE) is also a potential green corrosion inhibitor due to it contains many active ingredients [16], some of which are shown in Fig. 1.

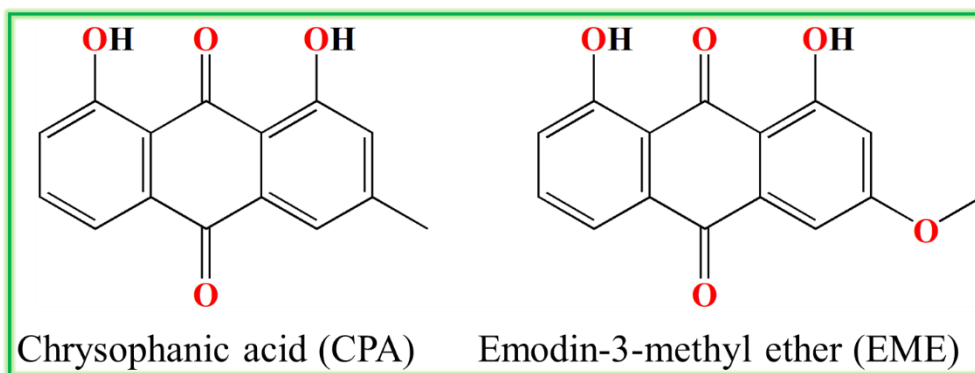


Figure 1. The CPA and EME molecular structure in Betel nut shell extract.

As we all know, no work was focused on BNE inhibition for the metal in a harsh acid solution. Herein, we prepared BNE extract via a water extraction method. Combined with electrochemical tests, gravimetric measurements, morphology observations, adsorption model, and theoretical calculations, we evaluated the anti-corrosion ability and absorption mechanism of BNE on Q235 steel in 1 M HCl. Ultimately, we hope this work can accumulate experience for the industrial application of plant extractant corrosion inhibitors.

2. EXPERIMENTAL

2.1 Materials

Q235 steel was purchased from the test piece processing center of Shengxin Corrosion Testing Equipment, Binzhou City, Shandong Province, China. The chemical element of Q235 steel was displayed in Table 1. The Q235 steel sample size for electrochemical tests, gravimetric measurements, and morphology observations was $1 \times 1 \times 1 \text{ cm}^3$. In addition, the sample used for electrochemical tests was sealed with a two-component adhesive (epoxy resin), retaining only one working surface ($1 \times 1 \text{ cm}^2$).

Table 1. The chemical element of Q235 steel.

Elements	P	Si	Ni	Mn	C	S	Cr	Cu	Fe
Proportion (%)	0.016	0.07	0.01	0.28	0.18	0.006	0.02	0.05	0.368

2.2 Preparation of BNE and test solution

Betel nut shell was collected in wanning City, Hainan Province, China. Based on the modified extraction method of Keramatinia [17], we prepared betel nut shell extract (BNE). First, betel nut shell was washed several times with deionized water to remove impurities. Then, the betel nut shell was dried at 373 K for 24 h. Next, a small pulverizer pulverized the dehydrated betel nut shell into powder. Afterward, betel nut shell powder was added to a beaker containing 1.5 L of deionized water and stirred (800 r/min) at 353K for 48 h. Next, the betel nut shell extract was filtered, centrifuged, and freeze-dried for 48 h. Finally, the yellow-brown betel nut shell powder was obtained and placed in a dry box.

The test solution was 1 M HCl, prepared from concentrated hydrochloric acid (37%, China Sinopharm Group) and deionized water. The added dosages of BNE in 1 M HCl were 50, 100, 300, and 500 mg/L.

2.3 Electrochemical test

All electrochemical experiments were tested via CHI 760E (China Shanghai Chenhua Instrument Co., Ltd.). The test three-electrode system included a working electrode ($1 \times 1 \text{ cm}^2$ Q235 steel), counter electrode ($1 \times 1 \text{ cm}^2$ Platinum net), and reference electrode (Saturated Calomel Electrode, SCE). After

completing the open circuit potential test, electrochemical impedance spectroscopy test (EIS) was carried out. The test frequency range for EIS was 10^5 Hz to 10^{-2} Hz, and the disturbance signal was a 5 mV sine wave. Afterward, the Polarization curve test was executed at 2 mV/s scanning rate within ± 250 mV versus open circuit potential. The whole electrochemical test was performed in a water bath at 25°C.

2.4 Gravimetric measurement and morphology observations

All samples used for gravimetric measurement and morphology observations were polished with sandpaper from 400 to 7000 mesh. Then, polished Q235 cubes were ultrasonically cleaned with ethanol and acetone. Next, they were dried via N_2 and weighed by an analytical balance. After being immersed in various concentrations of BNE for 4 h, all samples were subjected to the above procedure again. Finally, the weight loss and corrosion rate were calculated and discussed.

Scanning electron microscopy (FEI-SEM, Quanta FEG 250, USA) and laser scanning confocal microscopy (LSM700, Germany) were used to observe the corroded sample morphology with different concentrations of BNE (0 and 500 mg/L) protection.

2.5 Theoretical calculation

Based on Materials Studio (MS) software, the theoretical calculation (DFT) of this work was executed [18]. Two molecules (CPA and EME) from BNE were optimized via the B3LYP method within the DFT level with 6 311++G(d, p) basis set [19-21]. Electron cloud distribution of the lowest unoccupied molecular orbital (LUMO) and highest occupied molecular orbital (HOMO) was obtained. In addition, some crucial parameters were gained and discussed in depth.

3. RESULTS AND DISCUSSION

3.1 Polarization curve

The Polarization curve test is one of the most conventional electrochemical testing techniques for corrosion inhibitors. Herein, we adopt the polarization curve test to explore the anti-corrosion of BNE for steel. As shown in Fig. 2, the cathodic and anodic current densities of Q235 steel are enormous in 1 M HCl solution, indicating that the bare steel is difficult to resist the corrosion of HCl [22, 23]. All Polarization curves of Q235 steel shift downward when BNE is added to the acidic medium. Meanwhile, the shift of Polarization curve becomes more evident with the increase in BNE concentration. This finding indicates that BNE suppresses steel corrosion, and this protective effect is positively correlated with the concentration of BNE [24]. Compared with the cathodic and anodic branches of Q235 steel within BNE, we find that the protective effect of BNE on the steel anode is constant, but it increases on the cathodic with the increase of BNE.

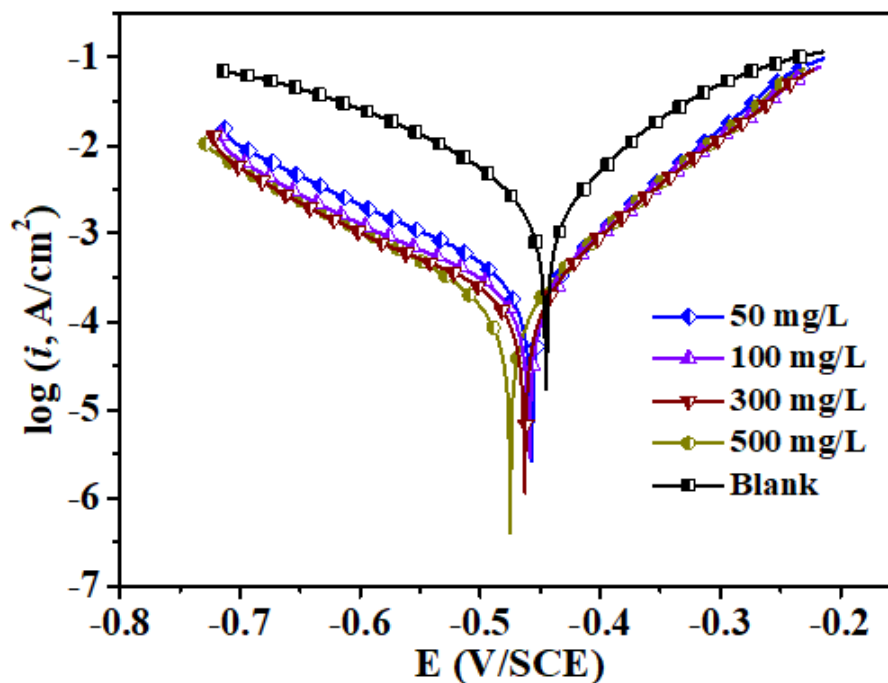


Figure 2. The Polarization curve of Q235 steel in 1 M HCl in presence of different concentrations of BNE

We used extrapolation to process the Polarization curves and further analyze the polarization data. Some crucial parameters are obtained and displayed in Table 2, such as E_{corr} , i_{corr} , cathodic and anodic polarization curve slopes (β_c and β_a), and η . Compared to the blank E_{corr} value, the biggest change of other E_{corr} values is 30 mV, which does not exceed 85 mV. Combined with the conclusions in Fig. 2, it can be concluded that BNE is a modest mixed-type corrosion inhibitor [25]. The blank i_{corr} value is 2.4 mA cm^{-2} , the highest among all the i_{corr} values. The value of i_{corr} decreases with the appearance of BNE. The minimum value of i_{corr} is 0.27 mA cm^{-2} when BNE is 500 mg/L. These phenomena show that BNE can form a shield film, isolating the contact between the steel and the corrosive media (Cl^- , H^+) [26]. Moreover, the protective film becomes denser with the increased concentration of BNE [27], which also explains why the η value increases with BNE concentration. Considering that the value of β_c and β_a is similar, the corrosion of Q235 steel in 1 M HCl solution is still a hydrogen evolution reaction [28].

Table 2. Potentiodynamic polarization parameters of Q235 steel in 1 M HCl containing various concentrations of BNE.

C (mM)	E_{corr} (V/SCE)	i_{corr} (mA cm^{-2})	β_c (mV dec^{-1})	β_a (mV dec^{-1})	η (%)
Blank	-0.445	2.4	-113	96	–
50	-0.463	0.35	-105	86	85.4
100	-0.463	0.32	-124	89	86.7
300	-0.465	0.30	-104	95	87.5
500	-0.475	0.27	-112	92	88.8

3.2 EIS

The Nyquist, Bode, and Phase angle plots of Q235 steel in 1 M HCl within various concentrations of BNE are displayed in Fig. 3. As shown in Fig. 3b, the Nyquist plot consists of an imperfect arc, which corresponds to capacitive and charge transfer impedance. Compared with Figs. 3a and b, we can find that the appearance of BNE makes the diameter of the semicircle expansion. At the same time, the radius of the semicircle also increased with the BNE concentrations. These phenomena indicate that BNE improves the difficulty of charge transfer by building a protective film [29]. This protective film also becomes complete and dense with increased BNE concentration. However, the Nyquist plot at 500 mg/L BNE does not change much compared to 300 mg/L BNE, implying that 300 mg/L is more practical and economical.

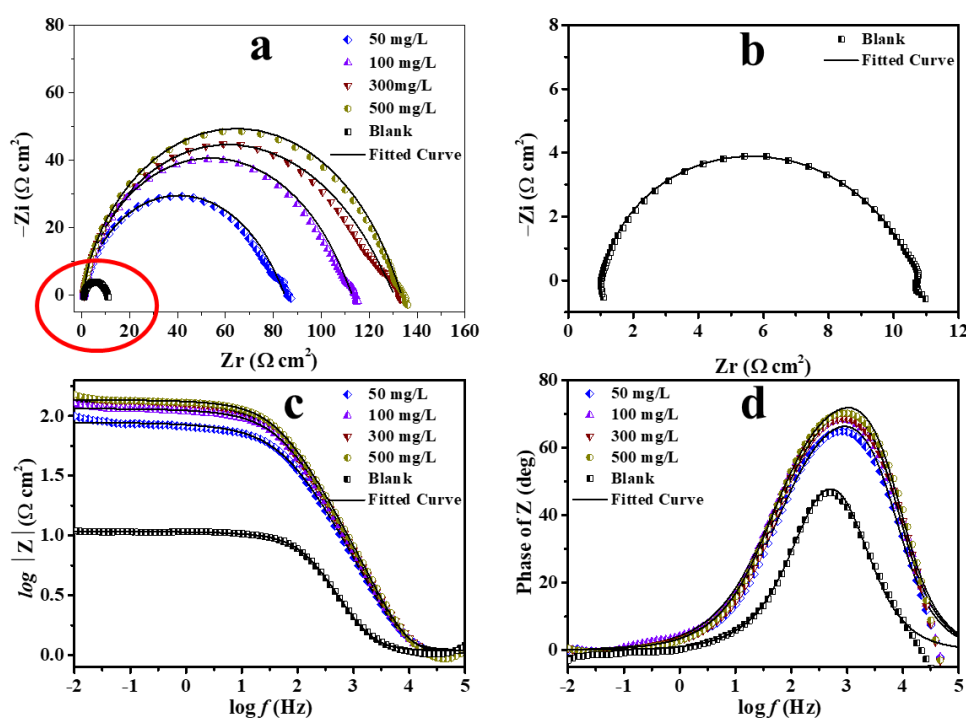


Figure 3. The EIS plots of Q235 steel within various concentrations of BNE, (a) Nyquist plot, (b) Partially enlarged view of (a), (c) Bode plot, (d) Phase angle plot.

The impedance modulus value of Q235 steel in Fig. 3c increases significantly after the appearance of BNE. Compared with blank, the impedance modulus value increases by nearly an order of magnitude when BNE concentrations exceed 100 ml/L. This finding demonstrates the protection of the Q235 steel by the BNE film. In addition, we observe a straight line between $\log f$ and $\log Z$ with a slope of about -1, which is a typical capacitive reactance behavior [30-32]. As shown in Fig. 3d, the appearance of BNE increases the maximum value and enhances the frequency range of the phase angle peak. These phenomena are consistent with the results obtained by Nyquist and Bode. However, only

one extreme peak is observed in the phase angle plot, possibly due to the coincidence of the two-time constant peaks.

We fit the EIS data to understand better the anti-corrosion ability of BNE for steel. The relevant equivalent circuit is shown in Fig. 4. Here, R_s is the solution impedance, R_f is the film impedance, R_{ct} is the charge transfer impedance, C_{dl} is the double-layer capacitance, and C_f is film capacitance [33]. These EIS parameters are displayed in Table 3. It can be seen from Table 3 that R_f and R_{ct} values enhance when BNE appearance. The total value of R_f and R_{ct} in blank solution is $9.6 \Omega \text{ cm}^2$, while the value is $139.9 \Omega \text{ cm}^2$ in 500 mg/L BNE. Obviously, under the protection of a high concentration of BNE, the impedance value of Q235 steel is increased by a hundred times.

However, the values of C_{dl} and C_f show an opposite trend to R_f and R_{ct} . The values of C_{dl} (from $95.1 \mu\text{F cm}^{-2}$ to $15.9 \mu\text{F cm}^{-2}$) and C_f (from $111.3 \mu\text{F cm}^{-2}$ to $21.4 \mu\text{F cm}^{-2}$) decrease rapidly with the increase of BNE, proving that BNE molecules replace corrosive ions (H^+ , Cl^-) and adsorb on steel. The highest value of η is 93.1% when the BNE concentration reaches 500 mg/L. This result is consistent with the Polarization curves conclusion, which proves that BNE can effectively inhibit steel corrosion.

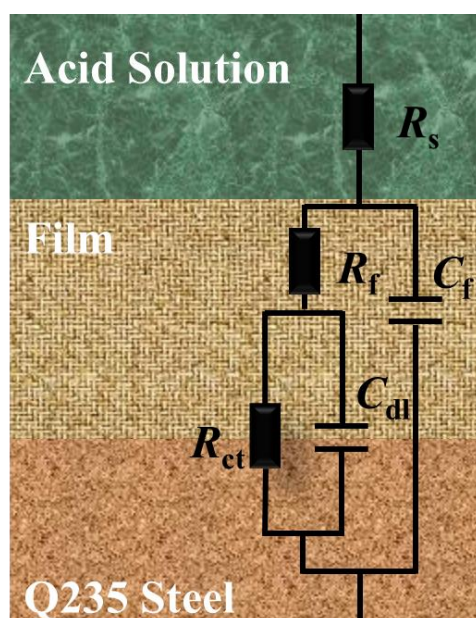


Figure 4. The relevant equivalent circuit used in our work.

Table 3. Some crucial EIS parameters of Q235 steel within various concentrations of BNE.

C (mg/L)	R_f (Ω cm^2)	R_{ct} (Ω cm^2)	C_f ($\mu\text{F cm}^{-2}$)	n_1	C_{dl} ($\mu\text{F cm}^{-2}$)	n_2	η (%)
Blank	3.8	5.8	95.1	1	111.3	0.69	-
50	8.5	78.7	21.6	1	35.5	0.58	89.0
100	14.5	101.3	19.2	1	24.1	0.60	91.7
300	17.1	112.8	17.3	1	22.6	0.58	92.6
500	24.2	115.7	15.9	1	21.4	0.63	93.1

3.3 Gravimetric measurements

The gravimetric measurements data of Q235 steel within various concentrations of BNE is given in Fig. 5. The corrosion rate of steel is $25.8 \text{ mg m}^{-2} \text{ h}^{-1}$, which is the highest in Fig. 5. When 50 mg/L BNE appears, the corrosion rate plummets to $4.5 \text{ mg m}^{-2} \text{ h}^{-1}$. Finally, the corrosion rate is only $2.9 \text{ mg m}^{-2} \text{ h}^{-1}$ when the BNE concentration is 500 mg/L. These findings suggest that a BNE film fabricates between the corrosion media and the Q235 steel substrate interface, inhibiting steel corrosion.

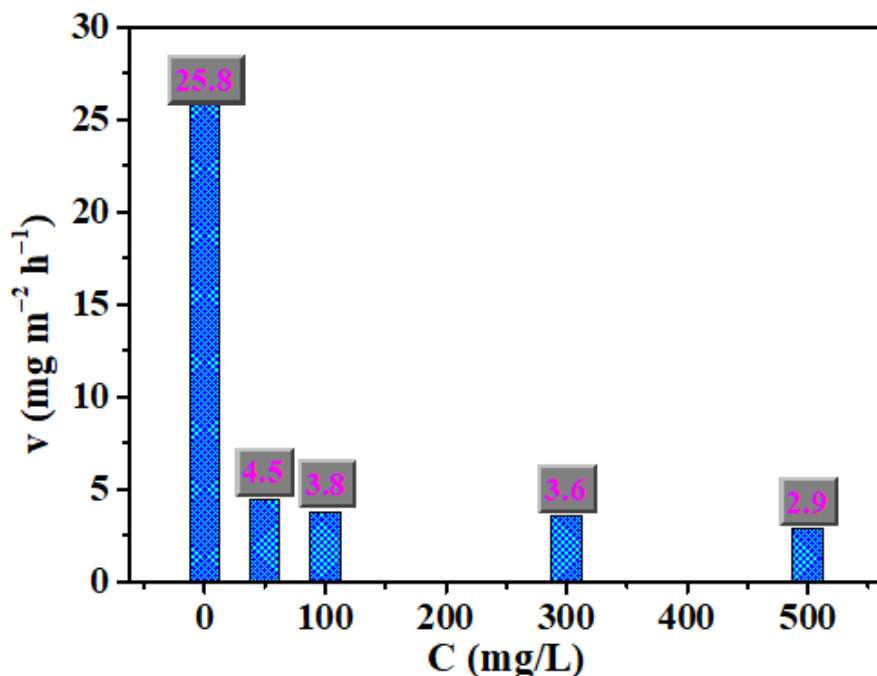


Figure 5. The gravimetric measurements data of Q235 steel within various concentrations of BNE.

3.4 Corrosion morphology

The 2D SEM and 3D LSCM plots of Q235 steel with 0 and 500 mg/L BNE are obtained in Figs 6 and 7. In Fig. 6a, the surface of Q235 steel has changed beyond recognition after being immersed in acid. Different corrosion products have covered the metal surface, consistent with Cui's results [34]. Due to the severe corrosion, corrosion pits and unevenness also appear on the metal surface. Obviously, it is difficult for Q235 steel to resist the attack of H^+ and Cl^- without protecting BNE. When 500mg/L BNE appears in the corrosive medium, the corrosion degree of Q235 steel decreases, as displayed in Fig. 6b. The entire metal matrix is visible in the SEM plot. However, some delicate corrosion areas are still observed on the metal surface. This phenomenon shows that even under the protection of BNE film, Q235 steel can still rust. Undeniably, the BNE film can greatly slow steel corrosion rate, which is also the fundamental reason for uncorroded areas on steel.

The 3D LSCM corrosion morphology is displayed in Fig. 6c. The corroded metal surface is exceptionally rough, with many bumps and depressions. Due to the accumulation of many corrosion

products on the surface, its average roughness (R_a) is as high as 1.83 μm . These observations are consistent with the SEM results, indicating that the Q235 steel is hardly resistant to attack from 1 M HCl. In contrast, the metal surface in Fig. 6d hardly sees the accumulation of corrosion products. Due to the existence of the BNE film, only some slight corrosion morphology is observed on the Q235 steel surface. In addition, the average roughness (R_a) also reduces to only 0.42 μm . The morphology observation proves the protective ability of BNE and is consistent with the result of other plant extract corrosion inhibitor [35].

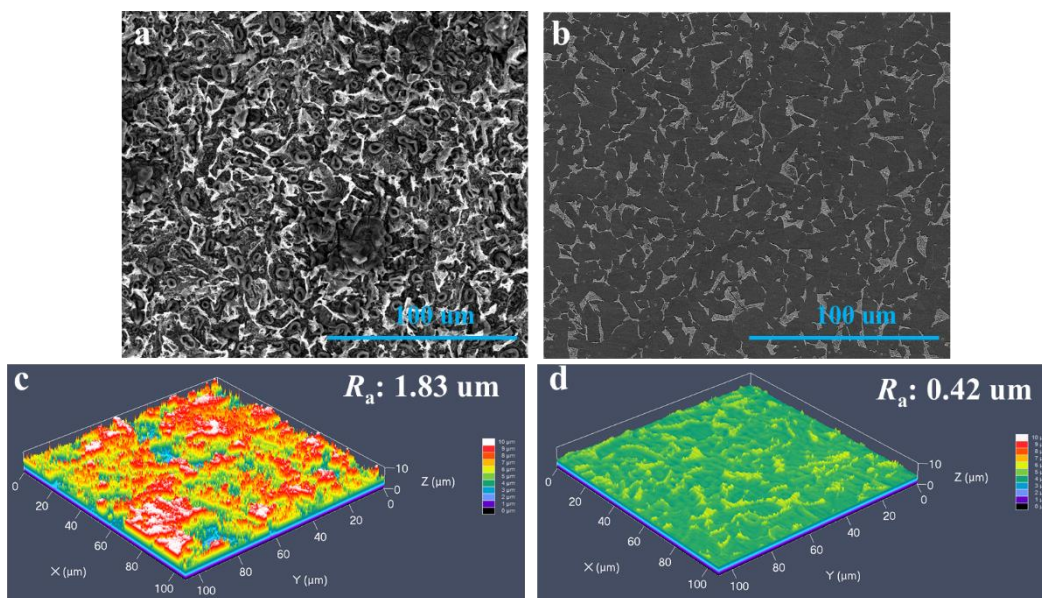


Figure 6. 2D SEM and 3D LSCM plots of Q235 steel with 0 and 500 mg/L BNE (a), (c) in 1 M HCl with 0 mg/L BNE, (b), (d) in 1 M HCl with 500 mg/L BNE.

3.5 Adsorption isotherm

Adsorption isotherm is used to explore the adsorption mechanism of BNE on Q235 steel in HCl solution. As shown in Fig. 7, the fitted R^2 value of Langmuir adsorption is 0.9999. It is reasonable to explain the adsorption mechanism of BNE molecules via the Langmuir adsorption isotherm. Based on Qiang's work [36], BNE molecules and corrosive ions have an equal chance of being adsorbed on the metal surface. Due to the high K_{ads} value (160.9 L/g), BNE molecules are more easily absorbed during competitive adsorption.

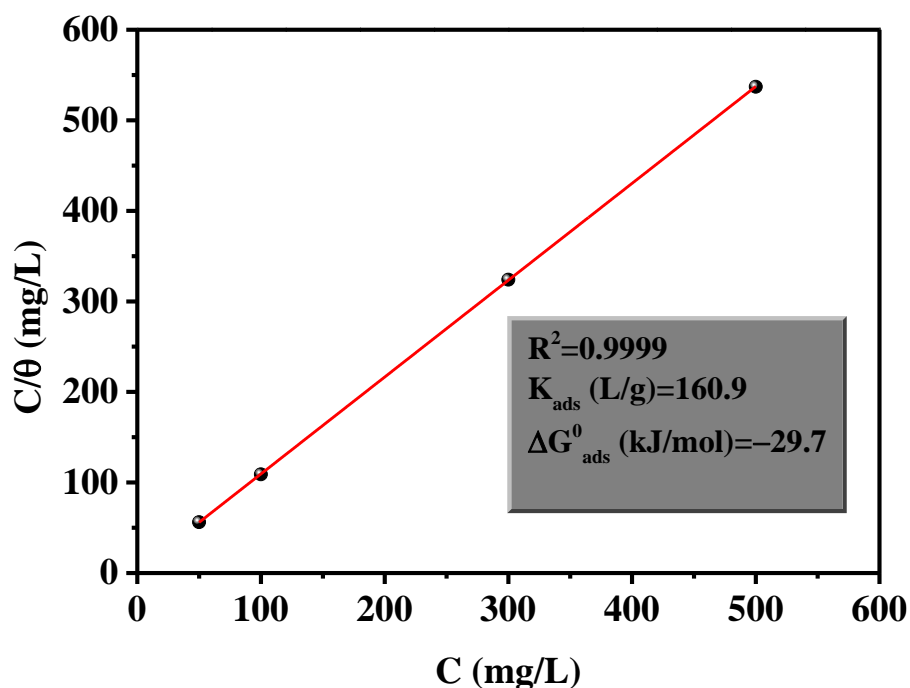


Figure 7. Langmuir adsorption isotherm and key thermodynamic parameters of Q235 steel with BNE.

Based on equations (1) and (2), two critical thermodynamic parameters (K_{ads} and ΔG_{ads}^0) are calculated and given in Fig. 7 [37].

$$\frac{C}{\theta} = \frac{1}{K_{\text{ads}}} + C \quad (1)$$

$$K_{\text{ads}} = \frac{1}{1000} \exp\left(-\frac{\Delta G_{\text{ads}}^0}{RT}\right) \quad (2)$$

Generally, when ΔG_{ads}^0 is negative, the entire reaction proceeds spontaneously. At the same time, when ΔG_{ads}^0 value is less than -40 kJ/mol, it can be regarded as chemisorption involving charge sharing or transfer between the studied inhibitor molecules and the metal [38]. While ΔG_{ads}^0 is more than -20 kJ/mol, it belongs to physisorption due to the electrostatic interaction between the charged metal and organic compounds [39]. In this work, the ΔG_{ads}^0 is -29.7 kJ/mol, proving that the adsorption of BNE is mixed-type with both physical and chemical adsorption. In addition, chemical adsorption is weaker than physical adsorption during the adsorption process.

3.6 Theoretical calculation

We selected two organic molecules (CPA and EME) in BNE and explored the distribution of their electron clouds in theoretical calculations. The structure, FMO distributions, and relevant quantum chemical parameters of CPA and EME are displayed in Fig. 8. As shown in Figs. 8a and b, the optimized 3D molecular structures of CPA and EME do not show obvious ectopic and are distributed in the same plane. This phenomenon indicates that CPA and EME (from BNE) possess parallel adsorption ability, which is also demonstrated in other work [40].

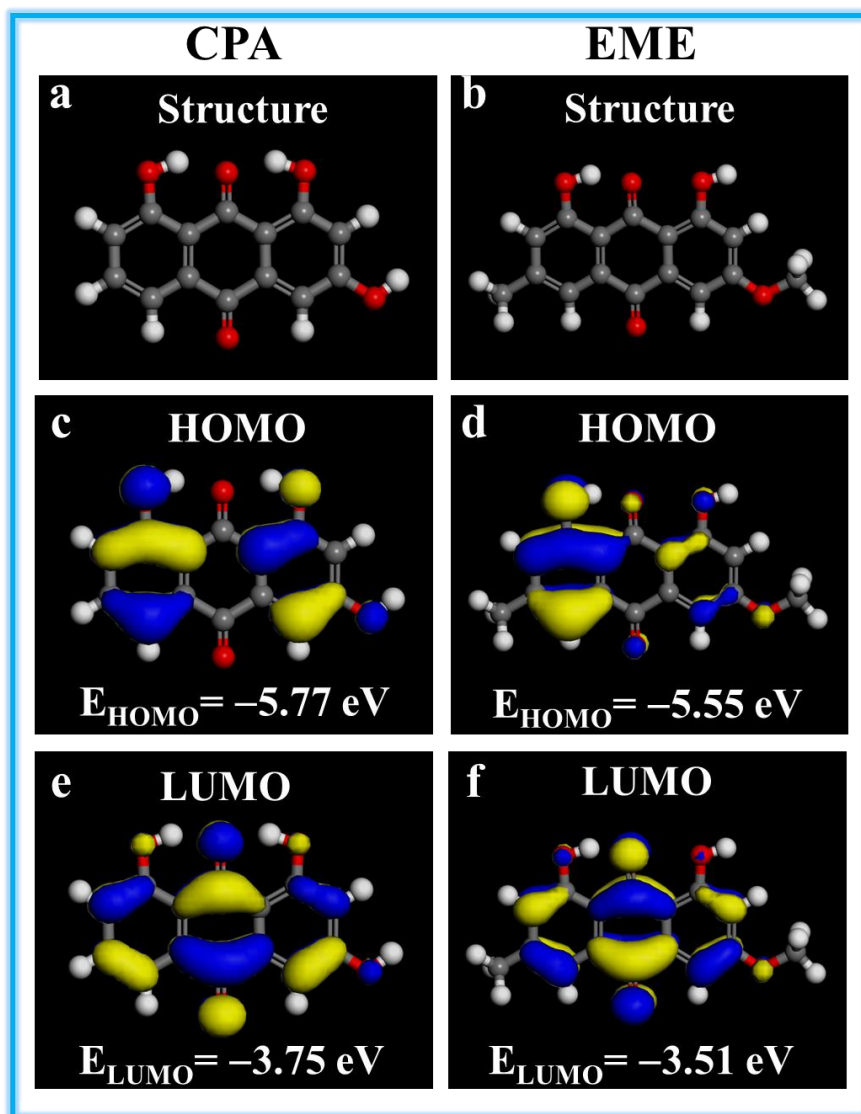


Figure 8. The structure, FMO distributions, and relevant quantum chemical parameters of CPA and EME.

The HOMO corresponds to donating electrons ability, and LUMO corresponds to receiving electrons ability [41]. For CPA, the HOMO electron cloud is dispersed on the left and right benzene rings, while the LUMO electron cloud is distributed on the whole molecule. For EME, the HOMO electron cloud is distributed only on the left benzene ring, while the LUMO electron cloud is distributed throughout the molecule. That is to say, both CPA and EME molecules can interact with the Q235 steel via donating or accepting electrons. Finally, BNE molecules can achieve parallel adsorption, thus reducing the contact area between the steel and the corrosive media [42]. Considering that the ΔE ($\Delta E = E_{\text{LUMO}} - E_{\text{HOMO}}$) value of CPA (2.02 eV) is similar to EME (2.04 eV), we believe that both CPA and EME molecules have incredible adsorption capacity and can provide supreme protection for steel in 1M HCl.

4. CONCLUSION

We prepared the betel nut shell extract (BNE) via the pure water extraction method. Based on experiments and theoretical calculations, we explored the anti-corrosion ability and adsorption mechanism of BNE to Q235 steel in 1 M HCl solution. Some crucial conclusions are shown as follows.

1. The polarization curve results indicate that BNE can slow the corrosion rate of Q235 steel by inhibiting its cathodic and anodic reactions. The anti-corrosion efficiency of BNE increases with BNE concentration.

2. Based on the EIS results, it finds that the appearance of BNE can significantly improve the film and charge transfer impedance of Q235 steel. At the same time, BNE can reduce film and electric double-layer capacitance. In 500 mg/L BNE solution, the η value is 93.1%.

3. We confirm that BNE can fabricate a protective film by combining gravimetric measurements and morphology observation. The BNE film provides a shield for Q235 steel in acid solution, reducing steel corrosion and roughness. Those results agree well with the above electrochemical results.

4. The adsorption mechanism of BNE molecules is explained via the Langmuir adsorption isotherm. Based on the thermodynamic parameters, it deduces that the adsorption of BNE belongs to physicochemical, while the physical adsorption is dominant.

5. From theoretical calculations, both CPA and EME molecules (from BNE) show potential chemical coordination ability with Q235 steel and can adsorb on the steel surface in parallel. Hence, a BNE film between the solution/steel interface will be built, reducing the contact area between the corrosive media and steel substrate.

References

1. H. Li, Y. Qiang, W. Zhao, and S. Zhang, *Corrosion Science*, 191 (2021) 109715.
2. Y. Qiang, L. Guo, H. Li, and X. Lan, *Chemical Engineering Journal*, 406 (2021) 126863.
3. S. Eid, *International Journal of Electrochemical Science*, 16 (2021) 150852.
4. B.R. Hou, X.G. Li, X.M. Ma, C.W. Du, D.W. Zhang, M. Zheng, W.C. Xu, D.Z. Lu, and F.B. Ma, *Npj Materials Degradation*, 1(1) (2017).
5. H. A. Alrafai, *International Journal of Electrochemical Science*, 17 (2022) 220216.
6. Y. Qiang, S. Zhang, and L. Wang, *Applied Surface Science*, 492 (2019) 228-238.
7. Z. Mirzakhazadeh, A. Kosari, M.H. Moayed, R. Naderi, P. Taheri, and J.M.C. Mol, *Corrosion Science*, 138 (2018) 372-379.
8. D.A. Winkler, M. Breedon, P. White, A.E. Hughes, E.D. Sapper, and I. Cole, *Corrosion Science*, 106 (2016) 229-235.
9. Y. Qiang, H. Li, and X. Lan, *Journal of Materials Science & Technology*, 52 (2020) 63-71.
10. D. Kumar, V. Jain, and B. Rai, *Corrosion Science*, 142 (2018) 102-109.
11. Y. Qiang, H. Zhi, L. Guo, A. Fu, T. Xiang, and Y. Jin, *Journal of Molecular Liquids*, 351 (2022) 118638.
12. T. Gu, Z. Chen, X. Jiang, L. Zhou, Y. Liao, M. Duan, H. Wang, and Q. Pu, *Corrosion Science*, 90 (2015) 118-132.
13. H. Li, S.T. Zhang, and Y.J. Qiang, *Journal of Molecular Liquids*, 321 (2021) 114450.
14. H. Li, Y.J. Qiang, W.J. Zhao, and S.T. Zhang, *Colloids and Surfaces a-Physicochemical and Engineering Aspects*, 616 (2021) 126077.
15. G. Bahlakeh, B. Ramezanzadeh, A. Dehghani, and M. Ramezanzadeh, *Journal of Molecular*

- Liquids*, 283 (2019) 174-195.
16. K. Kumpawat, S. Deb, S. Ray, and A. Chatterjee, *Mutation Research/Genetic Toxicology and Environmental Mutagenesis*, 538 (2003) 1-12.
 17. M. Keramatnia, M. Ramezanzadeh, G. Bahlakeh, and B. Ramezanzadeh, *Corrosion Science*, 178 (2021) 109077.
 18. H. Li, S. Zhang, B. Tan, Y. Qiang, W. Li, S. Chen, and L. Guo, *Journal of Molecular Liquids*, 305 (2020) 112789.
 19. Y. Qiang, S. Zhang, B. Tan, and S. Chen, *Corrosion Science*, 133 (2018) 6-16.
 20. Y. Qiang, S. Zhang, S. Xu, and W. Li, *Journal of Colloid and Interface Science*, 472 (2016) 52-59.
 21. E. Alibakhshi, M. Ramezanzadeh, S.A. Haddadi, G. Bahlakeh, B. Ramezanzadeh, and M. Mahdavian, *Journal of Cleaner Production*, 210 (2019) 660-672.
 22. J. Haque, V. Srivastava, M.A. Quraishi, D. Singh Chauhan, H. Lgaz, and I.-M. Chung, *Corrosion Science*, 172 (2020) 108665.
 23. X. Yao, Y. Qiang, L. Guo, Q. Xu, L. Wen, and Y. Jin, *Journal of Industrial and Engineering Chemistry*, 114 (2022) 427-437.
 24. J.J. Zhu, H. Hao, and X.W. Zheng, *International Journal of Electrochemical Science*, 17 (2022) 220321.
 25. W. Chen, and W.W. Xiao, *International Journal of Electrochemical Science*, 17 (2022) 220427.
 26. Q. Zhang, Z. Ye, Z. Zhu, X. Liu, J. Zhang, and F. Cao, *Corrosion Science*, 139 (2018) 403-409.
 27. Y. Qiang, S. Fu, S. Zhang, S. Chen, X. Zou, *Corrosion Science*, 140 (2018) 111-121.
 28. W. Su, B. Tang, F. Fu, S. Huang, S. Zhao, L. Bin, J. Ding, and C. Chen, *Journal of Hazardous Materials*, 279 (2014) 38-45.
 29. A. S. Mogoda, and K. M. Zohdy, *International Journal of Electrochemical Science*, 17 (2022) 22012.
 30. Y. Qiang, S. Zhang, H. Zhao, B. Tan, and L. Wang, *Corrosion Science*, 161 (2019) 108193.
 31. Y. Wu, W. Zhao, S. Liu, and L. Wang, *Chemical Engineering Journal*, 438 (2022).
 32. Y. Wu, W. Zhao, and J. Ou, Stable, *Advances in Colloid and Interface Science*, 295 (2021) 102494.
 33. Y. Zhang, Y. Qiang, H. Ren, J. Cao, L. Cui, Z. Zong, D. Chen, and T. Xiang, *Progress in Organic Coatings*, 170 (2022) 106971.
 34. S. Ren, M. Cui, X. Chen, S. Mei, and Y. Qiang, *Journal of Colloid and Interface Science*, 628 (2022) 384-397.
 35. V. Rajeswari, D. Kesavan, M. Gopiraman, P. Viswanathamurthi, K. Poonkuzhali, and T. Palvannan, *Applied Surface Science*, 314 (2014) 537-545.
 36. Y. Qiang, S. Zhang, S. Yan, X. Zou, and S. Chen, *Corrosion Science*, 126 (2017) 295-304.
 37. M. Jokar, T.S. Farahani, and B. Ramezanzadeh, *Journal of the Taiwan Institute of Chemical Engineers*, 63 (2016) 436-452.
 38. Y. Qiang, S. Zhang, S. Xu, and L. Yin, *RSC Advances*, 5 (2015) 63866-63873.
 39. P. Mourya, S. Banerjee, R.B. Rastogi, and M.M. Singh, *Industrial & Engineering Chemistry Research*, 52 (2013) 12733-12747.
 40. M.T. Majd, M. Ramezanzadeh, B. Ramezanzadeh, and G. Bahlakeh, *Journal of Hazardous Materials*, 382 (2020) 121029.
 41. M. Ramezanzadeh, G. Bahlakeh, Z. Sanaei, and B. Ramezanzadeh, *Applied Surface Science*, 463 (2019) 1058-1077.
 42. L. Guo, S. Kaya, I.B. Obot, X. Zheng, and Y. Qiang, *Journal of Colloid and Interface Science*, 506 (2017) 478-485